Assessment of particle size magnifier inversion methods to obtain particle size distribution from atmospheric measurements

Tommy Chan[1,2], Runlong Cai[1,2], Lauri R. Ahonen[2], Yiliang Liu[3], Ying Zhou[1], Joonas Vanhanen[4], Lubna Dada[1,2], Yan Chao[1,2],

5 Yongchun Liu[1], Lin Wang[3], Markku Kulmala[1,2], Juha Kangasluoma[1,2]

[1]Aerosol and Haze Laboratory, Beijing Advanced Innovation Center for Soft Matter Science and Engineering, Beijing University of Chemical Technology, Beijing 100029, China
[2]Institute for Atmospheric and Earth System Research / Physics, Faculty of Science, University of Helsinki, Helsinki 00014 Finland
10 [3]Shanghai Key Laboratory of Atmospheric Particle Pollution and Prevention (LAP[3]), Department of Environmental Science and Engineering, Fudan University, Shanghai 200433, China.
[4]Airmodus Ltd., Erik Palménin aukio 1, Helsinki 00560, Finland

Correspondence to: Tommy Chan (tommy.chan@helsinki.fi), Juha Kangasluoma (juha.kangasluoma@helsinki.fi)

Abstract. Determining the particle size distribution of atmospheric aerosol particles is an important component to understand
15 nucleation, formation and growth. This is particularly crucial at the sub 3 nm range because of the growth of newly-formed nanoparticles. The challenge in recovering the size distribution is due its complexity and the fact that not many instruments currently measure at this size range. In this study, we used the particle size magnifier (PSM) to measure atmospheric aerosols. Each event was classified into one of the three types: new particle formation (NPF), non-event and haze events. We then compared four inversion methods (step-wise, kernel, Hagen and Alofs and expectation-maximization) to determine its
20 feasibility to recover the particle size distribution. In addition, we proposed a method to pre-treat measured data and introduced a simple test to estimate the efficacy of the inversion itself. Results showed that all four methods inverted NPF events well; but the step-wise and kernel methods fared poorly when inverting non-event and haze events. This was due to their algorithm, such that when encountering noisy data (e.g. air mass fluctuations) and under the influence of larger particles, these methods overestimated the size distribution and reported artificial particles during inversion. Therefore, using a statistical hypothesis
25 test to discard noisy scans prior to inversion is an important first step to achieve a good size distribution. As a first step after inversion, it is ideal to compare the integrated concentration to the raw estimate (i.e., the concentration difference at the lowest supersaturation and the highest supersaturation) to ascertain whether the inversion itself is sound. Finally, based on the analysis of the inversion methods, we provide recommendations and codes related to the PSM data inversion.

1 Introduction

30

Gas-to-particle conversion proceeds via molecular clustering and subsequent cluster growth in various systems, such as atmospheric particle formation events, combustion processes or nanoparticle synthesis (Almeida et al., 2013; Carbone et al.,

2016; Fang et al., 2018; Feng et al., 2015; Jokinen et al., 2018; Kulmala et al., 2004; Sipilä et al., 2016). Gas phase cluster formation and growth occurs at the size of a few nanometers, and direct measurements are presently available to probe the

35   dynamics of the process. Instruments such as the scanning mobility particle sizer (SMPS; Wang and Flagan (1990)), particle size magnifier (PSM; Vanhanen et al. (2011)), neutral cluster and air ion spectrometer (NAIS; Mirme and Mirme (2013)) or the pulse height analysis condensation particle counter (PHA CPC; Marti et al. (1996)) have been previously applied to directly measure the formation and growth of the clusters (Cai et al., 2017; Jiang et al., 2011; Kontkanen et al., 2017; Manninen et al., 2010; Sipilä et al., 2009; Yu et al., 2017). These instruments have different operation principles and instrument functions, and

40   therefore need specific data inversion methods to obtain a reliable conversion from the measured (i.e., raw) data to a particle number size distribution. The SMPS, for instance, is a differential method, measuring a narrow size band at once time (Stolzenburg and McMurry, 2008). The PSM, on the other hand, is a cumulative method, which measures total particle concentrations above certain threshold diameters (Cai et al., 2018). The comparison of the size distributions measured by these and some other instruments reveal that there is still work required to improve the accuracy of the measured sub-10 or sub-3

45   nm size distributions (Kangasluoma et al., 2019). Our focus in this study is the data inversion of the PSM for applications in atmospheric measurements.

Particle detection in the PSM is based on condensational growth of particles in two separate stages. In the first stage, the particles are grown with diethylene glycol (DEG) up to around 100 nm by mixing heated DEG vapour with a sample flow. In

50   the second stage, the grown particles are further grown with butanol. The cut-off diameter (i.e., the diameter at which 50% of the particles are grown) in the first stage varies approximately between 1-3 nm, depending on the mixing ratio of DEG vapour. The mixing ratio is controlled by varying the flow rate that is saturated by DEG. Therefore, the raw data for the inversion problem is the measured total particle concentration above a certain cut-off diameter as function of the flow rate through the saturator. Several parameters need to be considered in this specific inversion problem: 1) the shape of the cut-off curves

55   (instrument size resolution); 2) the data pre- and post-treatment to minimize random noise in the data; and 3) the mathematical method for the inversion.

To retrieve the sub-3-nm aerosol size distributions from the PSM raw data, the step-wise method and the kernel function method (Lehtipalo et al., 2014) have been used for PSM data inversion of atmospheric measurements. The step-wise method

60   is the promoted inversion method for commercial PSMs and supported by the manufacturer. It neglects the impact of the limited size resolution of PSM to the measured aerosol concentration at each saturation flow rate, and hence, causes systematic biases. The kernel function method considers the finite size resolution during inversion; however, it is more sensitive to random uncertainties than the step-wise method. To improve PSM inversion, Cai et al. (2018) compared four inversion methods: the step-wise method, the kernel function method, the Hagen-Alofs (H&A) method (Hagen and Alofs, 1983), and the expectation-

65   maximization (EM) algorithm (Hagen and Alofs, 1983; Maher and Laird, 1985). It was suggested that the EM algorithm considers the finite size resolution and is less sensitive to random errors compared with the kernel function and H&A methods.

However, the study by Cai et al. (2018) was mainly based on theoretical simulations and well-controlled laboratory experiments. For real atmospheric measurements, the larger measurement uncertainties compared to laboratory experiments may pose a challenge for each of these inversion methods. As indicated in Cai et al. (2018), the random uncertainty of the inverted size distribution is significant even under a relative uncertainty of 10% in the raw data. Furthermore, different from lab experiments in which the detection efficiency for each particle size is known, the PSM detection efficiency of atmospheric aerosols are not determined due to their unknown chemical compositions. This unknown detection efficiency may also cause non-negligible biases (Kangasluoma and Kontkanen, 2017) to the inverted PSM data. As a result, the feasibility and performance of these inversion methods need further verification and testing using the atmospheric measured data.

In this study, we present the four methods to invert measured, atmospheric PSM data obtained in Beijing, China. We discuss the following protocol to obtain the particle size distribution: 1) the usability of individual scans; 2) the comparison of typical, inverted individual scans using the four inversion methods; 3) the characteristics of each inversion method when applied to atmospheric data; and 4) a simple method to determine, as a first approximate, the reliability of the inversion. Finally based on the analysis of the performance of the inversion methods, we provide recommendations on how to invert atmospheric data measured with the PSM.

2 Materials and Methods

2.1 Site Description

The study site is located on the fifth floor at the Aerosol and Haze Laboratory of the Beijing University of Chemical Technology, located at the Haidan District in Beijing, China (39° 56' 31" N, 116° 17' 49" E, and 58 m above sea level). The laboratory is near the 3rd ring road of Beijing and gives a good representation of an urban environment that is surrounded by traffic roads, highways, residential and commercial buildings. The combination of these different zones brings together pollution from local (e.g. traffic emissions, cooking) and neighbouring sources.

This study was conducted between 15 Jan. and 31 Mar. 2018 ($n = 76$ days) and was representative of a Beijing winter. Beijing winters are generally cold and dry, with an average temperature of 0°C. The average monthly temperature highs are 2°C, 5°C and 12°C, and monthly lows are -9°C, -6°C and 0°C in January, February and March, respectively. During these three months, the average humidity and rainfall was ~44% and 5.33 mm, respectively.

2.2 Classification of event types

100

Three event types were identified for the study: new particle formation (NPF), haze and non-event (i.e. neither haze nor NPF events). An NPF event is classified according to the method introduced by Dal Maso et al. (2005), such that the growth of particles increase in size across different modes over several hours. Haze events were identified as days when the relative humidity was lower than 80% and the visibility range was less than 10 km – for a duration of 12 continuous hours. During the

105   study period, we observed in total, 29 NPF, 36 haze and 11 non-events. NPF events were typically isolated as daily events that occurred after sunrise and continued to the early afternoon. Meanwhile, haze events occurred randomly throughout the day and could last for several days. These three event types did not commonly overlap one another during the study period.

2.3 Aerosol particle measurements

110   Aerosol particle number concentration, expressed in $\#/cm^3$, was measured using a butanol-based condensation particle counter (CPC; model A20, Airmodus Ltd., Finland). The CPC can measure maximally particle concentration upwards to 10^5 $\#/cm^3$. The CPC is connected directly to the Particle Size Magnifier (PSM; model A10, Airmodus Ltd., Finland). The PSM is a pre-conditioner for the CPC that uses diethylene glycol as the working fluid to activate and grow nano-sized particles (~1-3 nm) so that can they be detected with the CPC (Vanhanen et al., 2011). A 1.3 m long horizontal inlet from where the aerosol

115   particles entered was fixed at the end of the PSM inlet and a core sampler was fitted to reduce sampling line losses (Fu et al., 2019; Kangasluoma et al., 2016). Losses due to particle diffusion, penetration and core sampling were accounted for after the data inversion. To maintain brevity, the term PSM will be used henceforth to refer to the PSM or the combination of CPC and PSM.

120   The PSM measures the total particle concentration by mixing sample aerosol flow with heated saturated flow containing diethylene glycol. By varying the saturator flow rate, the mixing ratio of the sample flow and saturated flow changes, thus particle cut-off size can be changed. In other words, particles of specific diameters assuming constant composition will be activated and grow to larger sizes based on the mixing ratio. In practice, the PSM can operate by scanning (i.e., incrementing followed by decrementing continuously) the saturator flow from 0.1-1.3 liters per minute (lpm) to vary the particle cut-off

125   size. The detection efficiency of the PSM as a function of the saturator flow rate is close to a sigmoid function, for which inversion methods taking into account the instrument function is needed. In this study, we adjusted the duration of each scan to be 240 seconds, recording data at one-second intervals.

2.4 Data pre- and post-treatment

130

During the process of converting the measured data into a particle size distribution, the data was checked and treated prior to inversion (pre-treatment) and following inversion (post-treatment). The programming language used for all data handling and

data analyses was MATLAB ver. R2019a (The Mathworks, Inc.). Because of fluctuations in the air masses, the measured concentration as a function of the supersaturation is not always monotonically increasing, making the inversion procedure

135   mathematically unsound. Further, during periods when no sub-3 nm particles are present, theoretically the measured concentration should be constant as a function of the supersaturation. Therefore, it is sensible to discard any scans not showing a positive correlation between the supersaturation and measured concentration to avoid inversion of any artificial counts from scans when there is clearly no sub-3 nm particles present – or if their presence is dubious.

140   The pre-treatment included a data quality check and noise removal procedure. As there is a general, near-linear relationship between the saturator flow rate and measured concentration, the quality check employed a statistical hypothesis test (Spearman's rank correlation coefficient) for each scan that retained scans considered significant and positive, while discarding scans considered contrary to retained scans. A statistical significance was set at $p < 0.05$ (as opposed to $p < 0.01$) to consider subtle changes, which could be a real atmospheric influence. Following the significance test, a locally weighted scatterplot

145   smoothing filter (LOWESS) was used over a span of six seconds for each single scan. The purpose of the smoothing was to minimize fluctuations or noise – for example, due to sudden changes in air mass. We explored the performance of the pre-treatment quality scan, especially pertaining to what scans were retained and discarded. In addition, we applied each inversion method to these retained and discarded scans to further understand the inversion process. A smoothing average over two scans (i.e. eight minutes in this study) was applied after the inversion. This reduced the random uncertainty in the inverted data and

150   facilitates, for example, the calculation of particle growth and formations rates. The smoothing is done after rather than before the inversion because the measured concentration is autocorrelated, whereas the inverted size distribution is simply a function of particle diameter and, therefore, can be averaged for the same size bin.

155   **2.5 Data inversion**

In this study, four inversion methods were tested using the data obtained in atmospheric measurements: the step-wise method (Lehtipalo et al., 2014), kernel function method (Lehtipalo et al., 2014), Hagen and Alofs method (H&A; Hagen and Alofs (1983)) and the expectation and maximization algorithm (EM; Dempster et al. (1977); Maher and Laird (1985)).

160
The particle number concentration measured with the PSM uses the Fredholm integral equation of the first kind to determine the particle size distribution:

$$R_i = \int\limits_0^{+\infty} \eta\left(s_i, d_\mathrm{p}\right) \times n \times \mathrm{d}d_\mathrm{p} + \varepsilon_i, \tag{1}$$

165   where R_i the particle number concentration when at the saturator flow rate is at s_i; η is the detection efficiency calculated from s and d_p; d_p is the particle size; $n(dd_p)$ is the particle size distribution function (units: particles/cm³); and ε_i are the errors in the measurement at s_i. For atmospheric measurements, the relatively large ε_i poses a challenge to data inversion.

The step-wise method is currently the proprietary inversion method for use with the PSM. When calculating particle size
170   distributions using the step-wise method, the size resolution of the PSM is assumed to be infinite (i.e., the kernel function is approximated with a Dirac delta function whose area is equal to the real kernel but height is infinite). Based on this assumption, it can be demonstrated that there is a one-to-one relationship between the saturator flow rate and the activated particle diameter, hence the particle number concentration in the specific size range can be obtained by calculating the measured particle number concentration increment (after correcting the detection efficiency) in its corresponding saturator flow rate range. The
175   expression for the stepwise method in practical use is:

$$n_m = \frac{2(R_{i+1} - R_i)}{\eta(s_{max}, d_i) + \eta(s_{max}, d_{i+1})} \times \frac{1}{d_i - d_{i+1}}, \tag{2}$$

where n_m is the particle size distribution (dN/dd_m) at diameter d_m; d_m is the median diameter of d_i and d_{i+1}; d_i and d_{i+1} are the corresponding diameter of saturator flow rates s_i and s_{i+1}, respectively, and this one-to-one relationship is obtained based on
180   the infinite-resolution assumption; R_i and R_{i+1} are the raw concentration recorded by the PSM and dilution has been corrected; s_{max} is the maximum saturator flow rate; and η is PSM detection efficiency at the given saturator flow rate and particle diameter. The inverted dN/dd_m was later converted into $dN/d\log d_m$.

The kernel function and H&A methods both account for the kernel functions of the PSM. At each saturator flow rate, the
185   measured total particle number concentration (or its derivative with respect to the saturator flow rate) is equal to the sum of particle number concentrations in each size bin multiplied by their detection efficiencies (or correspondingly kernel functions). The particle number concentrations in each size bin are obtained by solving the non-homogeneous, linear equations that relate saturator flow rates and particle number concentrations. The difference between the kernel function and the H&A methods is the number of assumed particle size bins. The kernel function method uses a size bin number (typically four to six) much less
190   than the number of saturator flow rates, while the H&A method uses a size bin number (theoretically infinite) much more than the number saturator flow rates and then reduces the size bin number to the saturator flow rate number using predetermined interpolation functions. Note that the H&A method itself does not specify that either the detection efficiencies or the kernel functions should be used for data inversion. In this study, detection efficiencies are used in the H&A method to avoid any uncertainties introduced when estimating the derivate of particle number concentration with respect to saturator flow rate; and
195   to keep in accordance with Cai et al. (2018).

The EM algorithm is an iterative algorithm based on the theories of probability, which is used in the inversion of diffusion batteries (Maher and Laird, 1985; Wu et al., 1989) and machine learning (e.g., Erman et al., 2006). The expressions for the EM algorithm are:

200

$$R_{i,j} = \frac{n_j \times \eta(s_i, d_j) \times \Delta d_j}{\sum_{j=1}^{J} n_j \times \eta(s_i, d_j) \times \Delta d_j}, \tag{3}$$

$$n_j = \frac{\sum_{i=1}^{I} R_{i,j}}{\sum_{i=1}^{I} \eta(s_i, d_j) \times \Delta d_j}, \tag{4}$$

where I is the total number of saturator bins and the ith saturator flow rate is s_i; J is the total number of particle size bins and the jth particle size is d_j; Δd_j is the width of the jth size bin; n_j is the particle size distribution at d_j (dN/dd_j); η is the PSM detection efficiency for the given s_i and d_j; $R_{i,j}$ is the contribution of the jth size bin to the total raw counts (R_i) measured at s_i and it is a

205 latent variable that cannot be directed measured. Similar to the H&A method, J should theoretically be infinite to avoid integral error caused by limited number of size bins and it is practically determined as 50 in this study. For additional details on the four inversion methods, refer to previous studies (Cai et al., 2018; Hagen and Alofs, 1983; Lehtipalo et al., 2014; Maher and Laird, 1985).

210 **2.6 Data Analysis**

With the study duration amounting to 76 days, we selected a total of 12 days for in-depth analysis: four days with an NPF event, four haze days and four non-event days. For the convenience of comparison, the aerosol size distributions from all the inversion methods are reported in six size channels. Six size channels were chosen because the six kernel function peaks do

215 not significantly overlap with each other (see SI, Fig. S1). The 6-channel distribution consisted of the following size range (nm): 1.2, 1.3, 1.5, 1.7, 2.0, 2.5 and 2.8 and the shape of the kernel was approximated with the Gaussian distribution. An 11-channel distribution was also estimated and was shown to be very similar to the 6-channel inversion (see SI, Fig. S1); nonetheless, the 6-channel distribution was used in this study as it is a commonly used size bin range. For the step-wise method, the total particle concentrations measured at 7 saturator flow rates were inverted into aerosol size distributions at 6 particle

220 sizes using Eq. (2). For the kernel function method, the measured particle concentration as a function of saturator flow rate was inverted to 6 aerosol size distributions using the least square method. For the H&A method and the EM algorithm, the size distribution was firstly inverted into 50 size channels and then reduced to 6 by merging adjacent channels. Assuming that there is no error or uncertainty in the kernel functions and particle aerosol number concentration recorded by the PSM, the inversion

methods should be able to distinguish more particle size channels even if their kernel function peaks may overlap with one
225 another or if size resolution is limited. However, considering the atmospheric instability and its particle composition is
unknown, we report the size distributions in six channels in this study.

The general challenge in the current sub-3 nm atmospheric size distribution measurements is that there is no real reliable
reference to compare size distributions. In some recent unpublished experiments, there has been a concurrent SMPS-based
230 measurement with the PSM; however, it only gives another independent estimate for the size distribution. Therefore, as a basis
of comparison between each inversion method, we compared the integrated total concentration from the inverted distribution
to the estimated raw concentration between 1.2 and 2.8 nm, $R_{1.2\text{-}2.8}$. This is calculated as the difference between the total particle
concentrations measured at the lowest and highest saturator flow rate (i.e., 0.1 lpm and 1.3 lpm). From this comparison, $R_{1.2\text{-}2.8}$ should be approximately equal to the inverted concentration. While the comparison is not expected to yield exact quantitative
235 agreement, it gives an idea of whether the inverted concentration is reasonable, especially during periods when little or no sub-
3 nm particles are present. Moreover, this comparison can ensure that the data is internally consistent.

The general workflow to obtain the particle size distribution using the PSM was as follows:

240   1) Pre-treat the data to remove scans with no statistical significance
      2) Select a smoothing method to remove random noise in the measurements
      3) Invert the measurement data
      4) Correct data for losses
      5) Apply a post-inversion smoothing
245   6) Compare the inversion to $R_{1.2\text{-}2.8}$ to check reliability of the inversion

In the following sections, we will first discuss the data pre-treatment, especially the criterion to retain and discard scans.
Following that, an overview of the four inversion methods applied on three event types will be shown. These results will be
inter-compared based on the sum of the inverted aerosol concentration and the aerosol size distributions in each size bin.

250 **3 Results**

3.1 Data retention rate and pre-inversion treatment

Table 1 presents the *p*-value statistical significance test to specific event days, with the total number of daily scans (from 00:00
to 23:59) and the number of retained and discarded scans. The test showed that both non-event and NPF events had a retention
255 rate over 90%, while haze events revealed an 80% retention rate. Of the three specific non-event days chosen, two had a high
retention rate, while one had as many discarded scans as a haze event. A typical example of a measured, four-minute scan can

be seen in Fig. 1. Retained scans (Fig. 1a and b) revealed a good correlation between the saturator flow rate and the measured particle concentration. In addition, the Spearman's rank correlation coefficient (ρ) of each retained scan was also significant. This contrasted discarded scans (Fig. 1c and d), which showed insignificant ρ with no correlation between the saturator flow rate and particle concentration.

Clearly, high retention rates indicate presence of sub-3 nm particles, while lower retention rates, such as during haze days, indicate that less sub-3 nm particles are present. As the aim is to invert high quality scans, only the scans with no significant correlation or negative correlation between the measured concentration and the saturator flow rate are discarded and, hence, the retention rate is around 80% even during haze days. However, the presence of sub-3 nm particles even in the presence of a high condensation sink also contribute to this high ratio of 80%, as discussed further in this study. Fig. 1c and 1d also present a typical challenge where the time resolution of the instrument (4 min. in this case) is larger than the time scale of the variations in the measured aerosol. High variations in the number concentration during one scan makes it oftentimes difficult to reliably invert data from a cumulative instrument, and indeed, the presented retention criteria may discard a large proportion of the scans that are mathematically difficult to invert.

3.2 Scan inversion

Individual, four-minute scans of both retained and discarded scans were inverted using the four inversion methods to assess the quality of the inversion and of the scan itself (Fig. 1). A measurable difference between retained and discarded inverted scans was observed. The inverted, discarded scans revealed little to no particle size concentration for each method, while inverted, retained scans revealed a quantifiable size distribution. From these inversions, one can make few observations. For example, all inversion methods give a rather similar-looking inverted size distribution for the retained scans, which suggests that all methods result in a reasonable inversion if the obtained raw data is good. This is in line the previous laboratory measurements by Cai et al. (2018). The exception is with the step-wise method, which is sensitive to the slight air mass fluctuations that may lead to negative inverted or erroneous concentrations in some size bins. In the selected examples of the discarded scans (Fig. 1c and 1d), the kernel and step-wise methods' inverted concentrations yielded a particle size distribution despite the scan suggesting to not have any signals from sub-3 nm particles. As indicated above, the observed concentration fluctuations may have originated from air mass fluctuations. This means that with the measurement uncertainties, the use of the step-wise and kernel methods without prior data checking may lead to the inversion of artificial particle concentrations that are only revealed during the inversion. On the other hand, the H&A and EM methods appear to be much more robust against noisy data; these methods inverted very little to no concentrations at all from the discarded scans. The significant differences in the behaviour of these inversion methods revealed measurement uncertainties that agree with the findings based on the Monte Carlo simulation in Cai et al. (2018).

3.3 Comparison of inversions to $R_{1.2\text{-}2.8}$ and total concentration

The inverted dataset was compared with $R_{1.2-2.8}$ of the same size range to estimate how well the inverted data is represented (Fig. 2). The variable $R_{1.2-2.8}$ is calculated as the particle concentration difference between saturator flow rate at 1.3 lpm and 0.1 lpm. The sub-3 nm particle concentration estimate based on $R_{1.2-2.8}$ was more reliable the larger the sub-3 nm particle concentration was relative to the background particle concentration. If the ratio is low, the sub-3 nm particle concentration

295 signal might not be distinguishable from the fluctuations of the background concentration. Further, since there are no corrections in the $R_{1.2-2.8}$ concentration estimate (e.g., losses), it might underestimate the real sub-3 nm particle concentration. During NPF events the step-wise inversion method reported the highest concentrations, about a factor of two larger than the kernel method, which showed the lowest concentrations. The H&A and EM methods reported concentrations were between the step-wise and the kernel method and closely resembled the concentration obtained from $R_{1.2-2.8}$. During non-NPF and haze

300 periods, such that when $R_{1.2-2.8}$ was very noisy, the kernel method revealed clearly the highest concentrations, which are likely due to overestimation. This was already observed in Fig. 1, where the kernel method-inverted concentrations were clearly inversion artefacts from scans that were discarded based on the insignificant correlation between the saturator flow rate and the measured particle concentration. The step-wise, EM and H&A methods showed rather similar concentrations, which were quite close to the values obtained from $R_{1.2-2.8}$ estimates. An interesting observation was during NPF events, where the H&A

305 and EM methods before and after the NPF revealed none to very little concentration, which is contrary to what the kernel and step-wise methods and $R_{1.2-2.8}$ estimates reported. This also could be observed during haze and non-event periods, but the differences are more subtle compared with the other inversion methods and $R_{1.2-2.8}$.

To get further insight into the overall performance of the inversions when the sub-3 nm particle concentration is low, histogram plots were made of the integrated concentration from the whole size range that is normalized with the total

310 concentration measured at the cut-off of 2.8 nm (0.1 lpm) (Fig. 3). Some observations can be made: the step-wise method is not sensitive to the concentrations because it is direct subtraction of concentrations; thus this may yield negative concentrations. The H&A and EM methods report high frequency at ~0, but also elevated frequencies below ratios less than 0.015 (or in absolute scale, less than about 200 cm^{-3}). This is in line with Cai et al. (2018), which show that the H&A and EM methods tend to report a near-zero size distribution when the sub-3 nm particle concentration is noisy and low compared to the

315 background aerosol concentration. There were some negative concentrations reported by the H&A and EM methods because we did not force the concentration to be non-negative (only for this comparison), thus $R_{1.2-2.8}$ showed negative values. In contrast, the kernel method never revealed ratios smaller than 0.015, which can be explained according to Figs 1c and 1d – even when inverting data that clearly does not contain a signal from sub-3 nm particles, the kernel method nevertheless inverted some artificial particle concentrations. These artificial inverted concentrations originate from the random noise in the data that

320 the inversion methods interpret as real signal.

3.4 Overview of inversion for different types of events

3.4.1 New Particle Formation events

All NPF events in the study showed a typical increase of particle concentration with the highest concentrations observed around
325 noon and minimally during the night (Fig. 4). All the methods revealed that the largest concentrations were observed in the
smallest size bin. The EM, H&A and kernel methods revealed high concentrations in the largest size bin. Both EM and H&A
methods showed very similar concentrations to one another. In contrast to the EM and H&A methods, the kernel and step-
wise methods revealed a larger total concentration outside of the NPF event and the concentration intensity revealed no
identifiable pattern. As discussed above, the difference is mainly caused by the behaviour of these inversion methods at a low
330 signal-to-noise ratio.

3.4.2 Non-events

During non-event days, there were no indication of NPF events (Fig. 4). The distribution of the EM and H&A methods looked
similar to each other in comparison with the kernel and step-wise methods. In addition, the H&A and EM methods revealed
335 no large particle sizes between 00:00–06:00 and 12:00–18:00, which largely contrasted the kernel and step-wise inversion
methods. The step-wise method revealed scattered gaps with no particle concentration throughout the day. This may be due to
the limitation of the step-wise inversion algorithm. Since the algorithm is calculated as the difference between two adjoining
size bins, if the difference is revealed as negative, the inversion itself would then have a gap in the size distribution. These
gaps are more evident during noisier periods, such as during haze and non-event types. In contrast, the size distribution are
340 latently smoothed in the H&A and EM methods.

Interestingly, all four inversion methods reported that there were constantly existing sub-1.7 nm particles with a clear diurnal
variation. This indicates that nucleation and initial growth of new particles occurred during the non-event period but were
scavenged by the background particles before growing into larger sizes. This is in agreement with the coagulation-controlled
345 particle growth mechanism after the formation of a $(H_2SO_4)_1(amine)_1$ cluster in urban Beijing (Cai et al., 2019), yet the source
and compositions needs to be further investigated.

3.4.3 Haze events

Similar to non-event days, the kernel and step-wise methods revealed particle concentrations in all size ranges throughout the
350 day, while the H&A and EM methods showed concentrations predominantly in the lower size range. This led to the latter two
methods being more qualitatively discernible compared with the kernel and step-wise methods. As with the other events, the
EM method had large concentrations of particles at the highest size bin.

355 3.5 Comparison of inversion size bins

To compare the single size bins of each inversion method, four size bins were selected: 1.2-1.3 nm, 1.5-1.7 nm, 1.7-2.0 nm and 2.0-2.5 nm (Fig. 5). Three days were chosen to represent NPF, non-event and haze days (see also Figs. 2 and 4). On the NPF event, all the four inversion methods captured the diurnal trend of particle size distribution initiated by NPF. Considering measurement uncertainties, the inverted size distribution from different inversion methods generally agreed well with each

360   other, although the kernel method reported much lower overall size distribution. As seen from Fig. 2, the kernel method inversion clearly underestimated the NPF event particle size distribution and is also revealed in Fig. 5 in all but the largest size bin. Meanwhile, the step-wise method reported higher aerosol size distributions compared with the H&A and EM methods. Although the 1.2-1.3 nm channel was very similar, the difference in measured concentration was attributed to other sizes – particularly between the sizes 1.5-2.0 nm. The largest size bin (2.0-2.5 nm) revealed an interesting observation, such that both

365   EM and H&A had lower concentrations compared with the step-wise and kernel methods. The latter two methods on 30 Jan showed a small peak at 07:00, which would be the approximate time that the NPF event begins (as seen in Fig. 2). It should be clarified that the true kernel functions are not determined due to the unknown aerosol chemical compositions. Hence, the differences between the inversion results may sometimes reflect the uncertainty of the measurement itself rather than simply quantify the difference of inversion methods.

370

On non-event and haze periods, newly formed clusters and particles are scavenged in a short period of time under the high coagulation sink in urban Beijing and their concentrations are presumably low (Cai et al., 2019). The EM method reported near-zero concentrations above 1.7 nm because it tends to report near-zero values when the particle concentration is low and noisy, as discussed in section 3.3. In contrast, the step-wise and kernel methods reported constantly existing concentration for

375   particles larger than 1.7 nm. The similar phenomenon was also observed during the midnight of the NPF event. The methodology biases, e.g., the infinite-resolution assumption of the step-wise method and the instability of the least square method used in the kernel and H&A methods are the major causes of the background. Although the methods each revealed inversion challenges with measured atmospheric data, it is important to note that in chamber studies (e.g., Cai et al. (2018)), the inversion methods were rather robust.

380

4 Summary and recommendations

In this study, we assessed the performance of four inversion methods: the step-wise, kernel, H&A and EM methods to invert PSM data measuring in real, atmospheric conditions. In addition, the study presented a novel method to pre-treat the data prior to inversion. The presented data employed a pre-treatment filter that scans the measured data to calculate the correlation

385   between the observed particle concentration and supersaturation of a single scan. From the correlation analysis, scans are discarded when there is a significant non-correlation or negative correlation. The performance of the inversion methods were assessed by inverting single scans. All the methods were found to perform relatively well for scans that were measured during new particle formation events, while the inverted size distributions were overestimated with the kernel method when the data is noisy (i.e., during non-event and haze periods), and negative values can be obtained with the step-wise method when

390 inverting noisy data. The EM and H&A methods were more robust when inverting noisy data, which in these cases, reported zeros. Since the variations in the background particle concentrations affected the performance of the inversion methods, one should be cautious when using any of these methods to appropriate a size distribution when the total measured concentration is less than ~500/cm^3 and a signal-to-noise ratio of ~0.02.

395 Based on the analysis presented in this study, we can make the following recommendations related to the PSM inversion procedure:

1) Data pre-treatment is an important part of the inversion to obtain reliable data. Scans that contain a clearly unphysical correlation between the measured concentration and supersaturation should be discarded.

400 2) As a first approximation, the PSM user should compare the inverted total sub-3 nm particle concentration to the sub-3 nm concentration obtained from the raw data by subtracting the concentration measured at lowest supersaturation from the concentration measured with highest supersaturation.

3) The kernel method should not be used to invert PSM data during a non-NPF event and used cautiously during NPF events. This is because inversions may be over- or under-estimated and at worst, artificial counts can be created by

405 the inversion itself.

4) The measured size distributions of ambient aerosols should be reported using a limited number of size bins (e.g., 4- to 6-channels) because the assumed inversion kernels may deviate from the true kernels.

5) The performance of the PSM should be checked regularly and the detection efficiency (that determines the inversion kernel) should be calibrated sporadically because the kernel information is used in the EM, H&A and kernel

410 inversions.

6) To improve data reliability, comparability and availability, the used inversion method and the measured size distribution functions ($\mathrm{d}N\mathrm{log}D_\mathrm{p}$ vs D_p) should be reported together with any other subsequent analysis from the PSM data.

7) The recommended method to retrieve the particle size distribution of PSM data is the EM method. However, it is

415 strongly advised to invert the data with another robust method, e.g., the step-wise method and to compare the results.

Table 1. List of selected days for analysis with their event type, number of scans and retention rate. All data are measured in 2018.

Event	Date (m/d)	No. of scans	Retained	Discarded
NPF	30 Jan	362	350	12
	31 Jan	359	336	23
	09 Feb	353	326	27
	16 Feb	357	321	36
Non-event	01 Feb	361	340	21
	13 Feb	361	296	65
	23 Feb	361	342	19
	06 Mar	361	283	78
Haze	17 Feb	361	285	76
	26 Feb	361	301	60
	02 Mar	361	283	78
	09 Mar	361	282	79

420
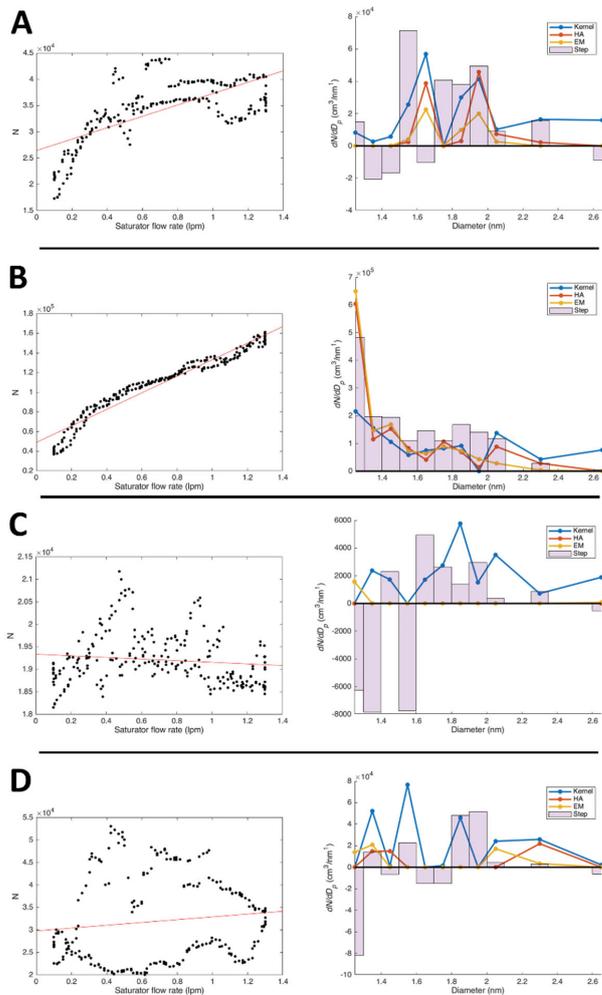
425

Fig. 1. Four individual, four-minute retained (a, b) and discarded (c, d) scans (left column) using the PSM and their inversion into a particle size distribution (right column). Note the difference in the (upward and downward) scan of the retained and discarded.

430
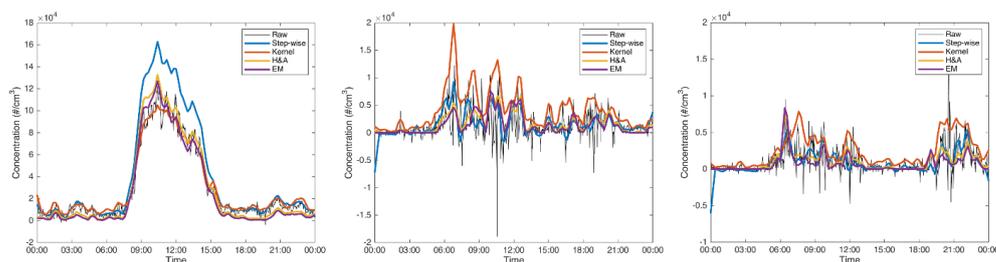
435

Fig. 2. Comparison of the inversions with raw (i.e, $R_{1.2\text{-}2.8}$; calculated as the difference between saturator flow rate at 1.3 lpm and 0.1 lpm). Event types shown are NPF (left; 30 Jan. 2018), non-event (center; 6 Mar. 2018) and haze (right; 9 Mar. 2018).
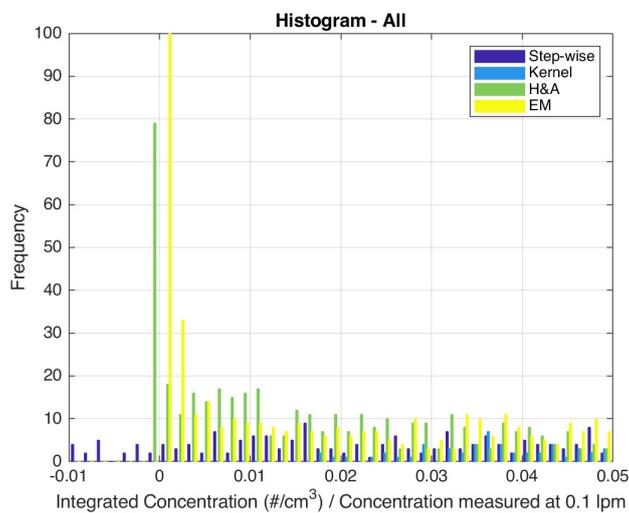
440

Fig. 3. Histogram plot of all selected study days. Data shown is the integrated concentration from the whole size range with the total concentration measured at the cut-off of 2.8 nm (0.1 lpm).

445
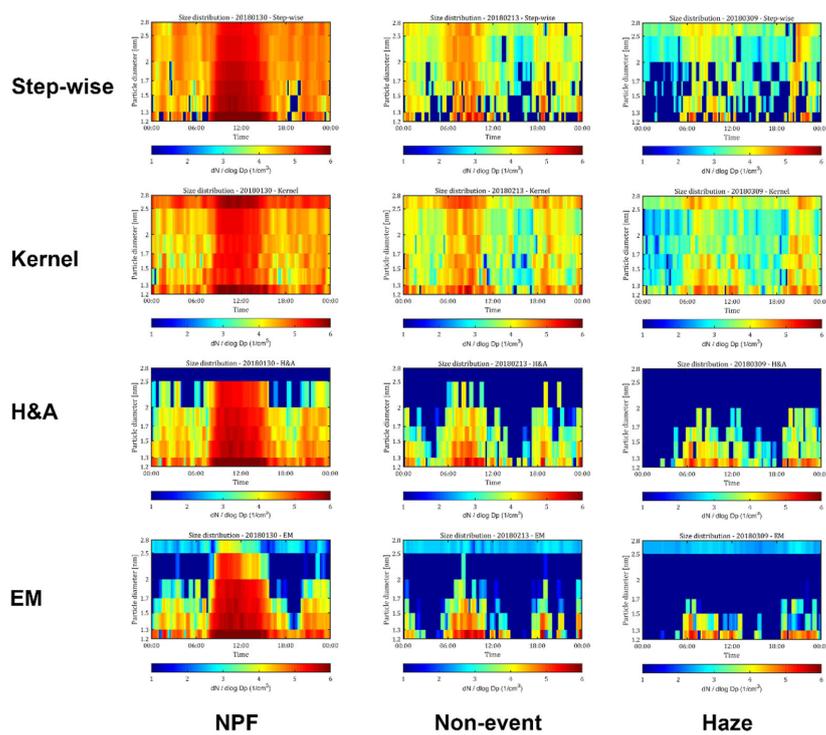
Fig. 4. Step-wise, kernel, H&A and EM inversions of a selected NPF (left; 30 Jan. 2018), non-event (center; 6 Mar. 2018) and haze
450 **(right; 9 Mar. 2018) event.**
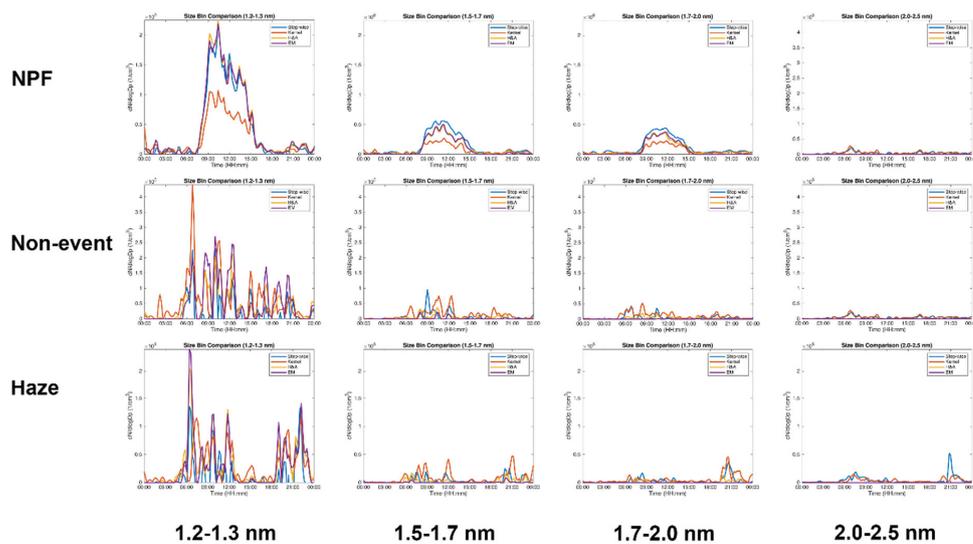
455

Fig. 5. Comparison of size bins from inversions. Event types shown are NPF (left; 30 Jan. 2018), non-event (center; 6 Mar. 2018) and haze (right; 9 Mar. 2018).

5 Code availability

460   MATLAB inversion codes used for this study are available via GitHub (https://github.com/tommychan-dev/PSM-Inversion).

6 Author contribution

TC, RC and JK designed the study and TC carried them out. TC, RC, LA, JV and LD developed the inversion code. YL (Fudan), LW, YZ, YC, YL (BUCT) and MK provided the facilities, instruments and funding for the study. TC prepared the manuscript with contributions from all co-authors.

465   ## 7 Competing interests

The authors declare that they have no conflict of interest.

8 Acknowledgements

This work was supported by the University of Helsinki, Faculty of Science support grant (#75284140), 3-year grant (#75284132) and the Finnish Academy of Science project (#1325656). MATLAB inversion codes are available via GitHub
470   (https://github.com/tommychan-dev/PSM-Inversion).

9 References

Almeida, J., Schobesberger, S., Kürten, A., Ortega, I. K., Kupiainen-Määttä, O., Praplan, A. P., Adamov, A., Amorim, A., Bianchi, F., and Breitenlechner, M.: Molecular understanding of sulphuric acid–amine particle nucleation in the atmosphere, Nature, 502, 359, 2013.

475   Cai, R., Jiang, J., Mirme, S., and Kangasluoma, J.: Parameters governing the performance of electrical mobility spectrometers for measuring sub-3 nm particles, Journal of Aerosol Science, 127, 102-115, 2019.

Cai, R., Yang, D., Ahonen, L. R., Shi, L., Korhonen, F., Ma, Y., Hao, J., Petäjä, T., Zheng, J., and Kangasluoma, J.: Data inversion methods to determine sub-3 nm aerosol size distributions using the particle size magnifier, Atmospheric Measurement Techniques, 11, 4477-4491, 2018.

480   Cai, R., Yang, D., Fu, Y., Wang, X., Li, X., Ma, Y., Hao, J., Zheng, J., and Jiang, J.: Aerosol surface area concentration: a governing factor in new particle formation in Beijing, Atmospheric Chemistry and Physics, 17, 12327, 2017.

Carbone, F., Attoui, M., and Gomez, A.: Challenges of measuring nascent soot in flames as evidenced by high-resolution differential mobility analysis, Aerosol Science and Technology, 50, 740-757, 2016.

Dal Maso, M., Kulmala, M., Riipinen, I., Wagner, R., Hussein, T., Aalto, P. P., and Lehtinen, K. E.: Formation and growth of
485   fresh atmospheric aerosols: eight years of aerosol size distribution data from SMEAR II, Hyytiala, Finland, Boreal
Environment Research, 10, 323, 2005.

Dempster, A. P., Laird, N. M., and Rubin, D. B.: Maximum likelihood from incomplete data via the EM algorithm, Journal of
the Royal Statistical Society: Series B (Methodological), 39, 1-22, 1977.

Erman, J., Mahanti, A., and Arlitt, M.: Qrp05-4: Internet traffic identification using machine learning, 2006, 1-6.

490   Fang, J., Wang, Y., Kangasluoma, J., Attoui, M., Junninen, H., Kulmala, M., Petäjä, T., and Biswas, P.: The initial stages of
multicomponent particle formation during the gas phase combustion synthesis of mixed SiO2/TiO2, Aerosol Science and
Technology, 52, 277-286, 2018.

Feng, J., Huang, L., Ludvigsson, L., Messing, M. E., Maisser, A., Biskos, G., and Schmidt-Ott, A.: General approach to the
evolution of singlet nanoparticles from a rapidly quenched point source, The Journal of Physical Chemistry C, 120, 621-630,
495   2015.

Fu, Y., Xue, M., Cai, R., Kangasluoma, J., and Jiang, J.: Theoretical and experimental analysis of the core sampling method:
Reducing diffusional losses in aerosol sampling line, Aerosol Science and Technology, 2019. 1-9, 2019.

Hagen, D. E. and Alofs, D. J.: Linear inversion method to obtain aerosol size distributions from measurements with a
differential mobility analyzer, Aerosol Science and Technology, 2, 465-475, 1983.

500   Jiang, J., Zhao, J., Chen, M., Eisele, F. L., Scheckman, J., Williams, B. J., Kuang, C., and McMurry, P. H.: First measurements
of neutral atmospheric cluster and 1–2 nm particle number size distributions during nucleation events, Aerosol Science and
Technology, 45, ii-v, 2011.

Jokinen, T., Sipilä, M., Kontkanen, J., Vakkari, V., Tisler, P., Duplissy, E.-M., Junninen, H., Kangasluoma, J., Manninen, H.,
and Petäjä, T.: Ion-induced sulfuric acid–ammonia nucleation drives particle formation in coastal Antarctica, Science
505   advances, 4, eaat9744, 2018.

Kangasluoma, J., Cai, R., Jiang, J., Deng, D., Stolzenburg, D., Ahonen, L., Chan, T., Fu, Y., Kim, C., Laurila, T., Y, Z., L, D.,
J, S., Flagan, R. C., Kulmala, M., Petäjä, T., and Lehtipalo, K.: Overview of measurements and current instrumentation for 1-
10 nm aerosol particle number size distributions Journal of Aerosol Science (submitted), 2019. 2019.

Kangasluoma, J., Franchin, A., Duplissy, J., Ahonen, L., Korhonen, F., Attoui, M., Mikkilä, J., Lehtipalo, K., Vanhanen, J.,
510   and Kulmala, M.: Operation of the Airmodus A11 nano Condensation Nucleus Counter at various inlet pressures and various
operation temperatures, and design of a new inlet system, Atmospheric Measurement Techniques, 2016. 2016.

Kangasluoma, J. and Kontkanen, J.: On the sources of uncertainty in the sub-3 nm particle concentration measurement, Journal
of Aerosol Science, 112, 34-51, 2017.

Kontkanen, J., Lehtipalo, K., Ahonen, L., Kangasluoma, J., Manninen, H. E., Hakala, J., Rose, C., Sellegri, K., Xiao, S., and
515   Wang, L.: Measurements of sub-3 nm particles using a particle size magnifier in different environments: from clean mountain
top to polluted megacities, Atmospheric Chemistry and Physics, 17, 2163-2187, 2017.

Kulmala, M., Vehkamäki, H., Petäjä, T., Dal Maso, M., Lauri, A., Kerminen, V.-M., Birmili, W., and McMurry, P.: Formation and growth rates of ultrafine atmospheric particles: a review of observations, Journal of Aerosol Science, 35, 143-176, 2004.

Lehtipalo, K., Leppa, J., Kontkanen, J., Kangasluoma, J., Franchin, A., Wimnner, D., Schobesberger, S., Junninen, H., Petaja, 520 T., and Sipila, M.: Methods for determining particle size distribution and growth rates between 1 and 3 nm using the Particle Size Magnifier, Boreal Environment Research, 2014. 2014.

Maher, E. F. and Laird, N. M.: EM algorithm reconstruction of particle size distributions from diffusion battery data, Journal of aerosol science, 16, 557-570, 1985.

Manninen, H., Nieminen, T., Asmi, E., Gagné, S., Häkkinen, S., Lehtipalo, K., Aalto, P., Vana, M., Mirme, A., and Mirme, 525 S.: EUCAARI ion spectrometer measurements at 12 European sites–analysis of new particle formation events, Atmospheric Chemistry and Physics, 10, 7907-7927, 2010.

Marti, J., Weber, R., Saros, M., Vasiliou, J., and McMurry, P. H.: Modification of the TSI 3025 condensation particle counter for pulse height analysis, Aerosol science and technology, 25, 214-218, 1996.

Mirme, S. and Mirme, A.: The mathematical principles and design of the NAIS–a spectrometer for the measurement of cluster 530 ion and nanometer aerosol size distributions, Atmospheric Measurement Techniques, 6, 1061-1071, 2013.

Sipilä, M., Lehtipalo, K., Attoui, M., Neitola, K., Petäjä, T., Aalto, P. P., O'Dowd, C., and Kulmala, M.: Laboratory verification of PH-CPC's ability to monitor atmospheric sub-3 nm clusters, Aerosol science and technology, 43, 126-135, 2009.

Sipilä, M., Sarnela, N., Jokinen, T., Henschel, H., Junninen, H., Kontkanen, J., Richters, S., Kangasluoma, J., Franchin, A., and Peräkylä, O.: Molecular-scale evidence of aerosol particle formation via sequential addition of HIO 3, Nature, 537, 532, 535 2016.

Stolzenburg, M. R. and McMurry, P. H.: Equations governing single and tandem DMA configurations and a new lognormal approximation to the transfer function, Aerosol Science and Technology, 42, 421-432, 2008.

Vanhanen, J., Mikkilä, J., Lehtipalo, K., Sipilä, M., Manninen, H., Siivola, E., Petäjä, T., and Kulmala, M.: Particle size magnifier for nano-CN detection, Aerosol Science and Technology, 45, 533-542, 2011.

540 Wang, S. C. and Flagan, R. C.: Scanning electrical mobility spectrometer, Aerosol Science and Technology, 13, 230-240, 1990.

Wu, J. J., Cooper, D. W., and Miller, R. J.: Evaluation of aerosol deconvolution algorithms for determining submicron particle size distributions with diffusion battery and condensation nucleus counter, Journal of aerosol science, 20, 477-482, 1989.

Yu, H., Dai, L., Zhao, Y., Kanawade, V. P., Tripathi, S. N., Ge, X., Chen, M., and Lee, S. H.: Laboratory observations of 545 temperature and humidity dependencies of nucleation and growth rates of sub-3 nm particles, Journal of Geophysical Research: Atmospheres, 122, 1919-1929, 2017.